



## CHAPTER II

### LITERATURE REVIEW

Corrosion is a concern for all nuclear plants. Corrosion produces deterioration of the material and its properties. Therefore, it has become an important issue for the operation of CANDU reactors. CANDU reactors, such as at Point Lepreau Generating Station (PLGS), are affected by excessive wall thinning rates within the outlet feeder pipes of the primary heat transport system.

#### 2.1 CANDU Nuclear Reactor

A CANDU reactor is a pressurized heavy water reactor (PHWR) that uses natural uranium as its fuel and heavy water (deuterium oxide) as its moderator. A schematic of a CANDU nuclear reactor illustrating these features is shown in Figure 2.1. Fuel bundles sheathed with zirconium alloy are contained in pressure tubes made of  $Zr2.5\%Nb$  passing horizontally through a vessel called the calandria containing a heavy water moderator. Heat from the nuclear reaction in the fuel bundles is removed by heavy water which is the primary coolant. This heat is carried by the heavy water through carbon steel pipes and headers to the steam generator where it is transferred to light (ordinary) water in the secondary cooling loop to produce steam. The steam is sent through a turbine which drives the generator producing electricity.

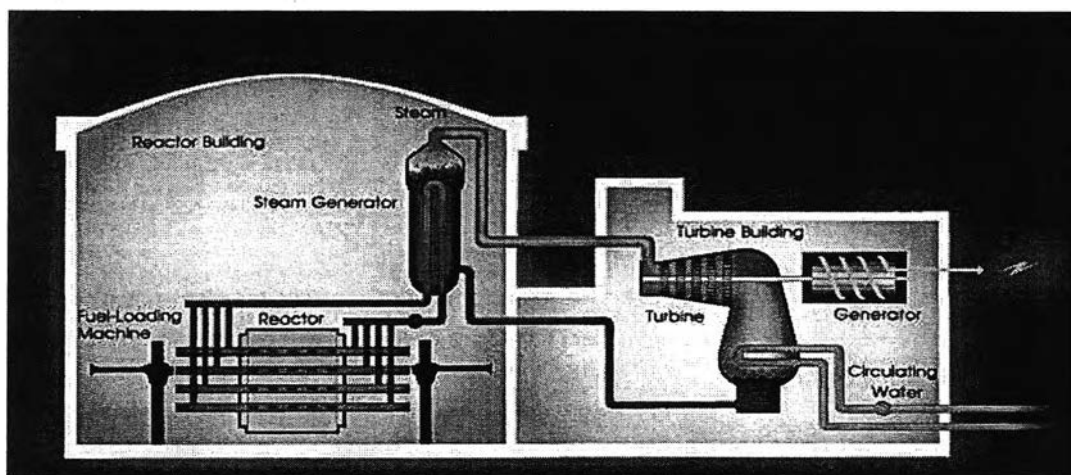
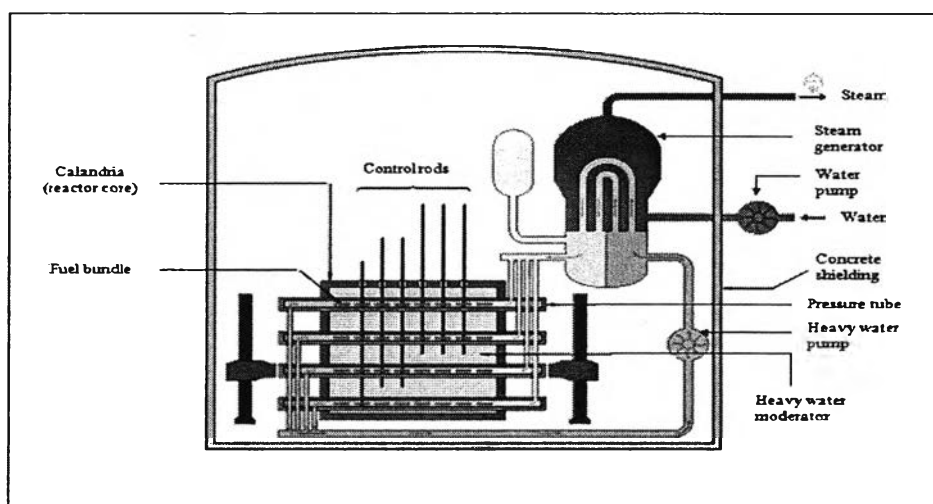


Figure 2.1 Schematic of a CANDU nuclear reactor (<http://www.nuclearfaq.ca>).

### 2.1.1 CANDU Primary Coolant Loop

Heavy water is the common name for deuterium oxide. It is similar to light water in many ways, except deuteriums replace the hydrogen atoms in water molecules to form heavy water ( $D_2O$ ) which is about 10 percent denser than light water and more viscous than light water. While the heavy water is expensive, the reactor can operate without enriched fuel thus balancing the costs.

The CANDU primary coolant loop contains three major components: the reactor core, the steam generator and the piping system as shown in Figure 2.2. The reactor core is a horizontal cylindrical tank called the calandria containing the heavy water ( $D_2O$ ) moderator which is maintained at about  $60^\circ C$ . The feeders, made of SA-106 Grade B carbon steel, carry the coolant directly into and out of the reactor fuel channels. The primary coolant  $D_2O$  enters the core at  $265^\circ C$  to remove heat from the nuclear reaction and leaves as a mixture of steam and water at  $310^\circ C$ . The mixture leaves the outlet feeders and headers and passes to the steam generators. The quality of the mixture increases slightly in transit because of the pressure drop along the piping. Average linear velocities of the coolant in the outlet feeders ranges from 8.0 m/s to 16.5 m/s. The alkalinity of the coolant is adjusted by ion-exchange in the purification system with lithium hydroxide to within the specified pH range of 10.3 to 10.8 at room temperature (Lister *et al.*, 1998).



**Figure 2.2** Schematic of primary coolant system of CANDU reactor (Emoscopes, 2006).

### 2.1.2 Materials and Conditions of Primary Coolant Loop

A summary of the material of construction of components in the CANDU primary coolant loop is shown in the following table, Table 2.1.

**Table 2.1** Material of construction of each component in primary coolant loop

Component	Material
Reactor core	Zirconium alloy 2.5%Nb
Steam generator*	Nickel alloy - Monel 400 - Inconel 600 - Incoloy 800
Piping	A-106 Grade B Carbon Steel

\* Depends on the CANDU model

The material of construction of the piping system is A-106 grade B carbon steel since it can withstand high temperatures and gives long term operation. Carbon steel A106 grade B pipe has iron as the main component with small amounts of other elements and is given in Table 2.1. The chromium concentration in the carbon steel is an important factor in the thinning phenomenon because chromium can form a protective oxide on the surface (Robertson and Forrest, 1991). Some recent work has focused on using coolant additives to lessen FAC. Bateman *et al.*, 2002 mentioned that from the early work at University of New Brunswick (UNB) had shown that a reduction in the corrosion rate was found to be 69% after titanium injection which forms an ilmenite film ( $\text{FeTiO}_3$ ) on the carbon steel surface which was adherent and protective. This film could withstand a jet impact of 20 m/s.

**Table 2.2** Chemical composition of A106 grade B carbon steel

Element	Mass fraction (%)
Fe	Balance
C	0.30
Mn	0.29
Si	0.10
S	0.04
P	0.04
Cr	0.03

The average primary heat transport system conditions over the normal range of operations are summarized in Table 2.3. It is under conditions of high temperature, high flow rates and low dissolved oxygen concentration that outlet feeders form their characteristic magnetite film. These conditions coupled with the under saturation of iron in the coolant, are believe to be sufficient to cause FAC and thereby produce hydrogen (Kelly *et al.*,2007).

**Table 2.3** Normal outlet feeder conditions at Point Lepreau Generating Station

Property	Normal value
Temperature	307-312°C Average: 310.7°C
Pressure	10.3 MPa
Two-phase quality	0.2-19% Average: 1.06%
Time in two-phase	0-94% Average: 49%
Average velocity	6.5-14.5 m/s Average: 12.2 m/s
pH <sub>a</sub>	Operating 10.2-10.4 since 1996
Dissolved O <sub>2</sub>	Specification < 0.01 mg/kg
Dissolved D <sub>2</sub>	Specification 3-10 mL(STP)/kg

## 2.2 Corrosion of Steel

### 2.2.1 Definition of Corrosion

Corrosion is defined as the destruction or deterioration of a material because of reaction with its environment. Higher temperatures and pressures usually involve more severe corrosion conditions leading to costly outages and repairs and can affect plant reliability and safety. However, corrosion is beneficial or desirable in some cases. For example, chemical machining or chemical milling, unmarked areas are exposed to acid and excess metal is dissolved. Anodizing of aluminum is another beneficial corrosion process used to obtain better and more uniform appearance in addition to a protective corrosion product on the surface (Mars G. Fontana, 1986).

### 2.2.2 Flow-Accelerated Corrosion (FAC)

Flow-accelerated corrosion (FAC), also known as flow-assisted corrosion, is the chemical dissolution of surface oxide and base metal, accelerated by flow and flow impingement. FAC can be anticipated whenever a susceptible metal is exposed to specific environmental conditions. The more important conditions are:

*Temperature:*

Studies on the effect of temperature on corrosion rate of mild steel have been performed in static aqueous solutions (Potter and Mann., 1962). Figure 2.3 shows that increased temperatures accelerate the corrosion of steel in 13 percent sodium hydroxide at 250-355°C.

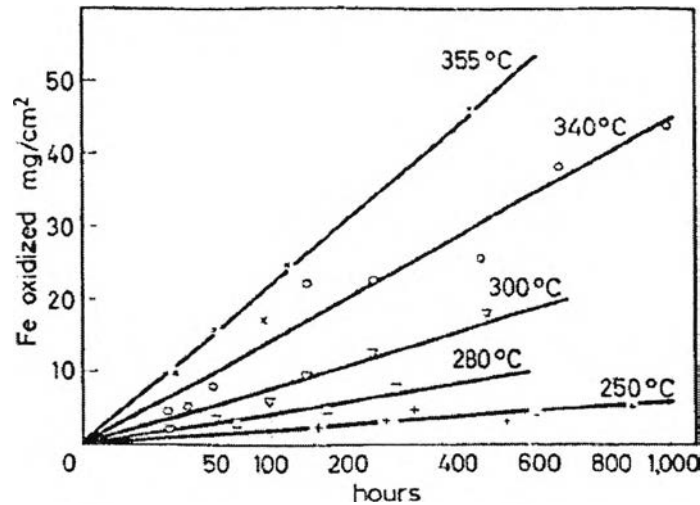


**Figure 2.3** Oxidation of mild steel in 13 percent sodium hydroxide at different temperature (Plotted against square root time).

Studies by Tomlinson and Ashmore done in 1986 show that carbon steel ferrules corrode significantly at 300°C with all volatile treatment water chemistry.

*pH:*

Carbon steel corrosion rates were measured in a refreshed autoclave impinging jet apparatus by Burrill and Cheluget (referenced in Corrosion of CANDU Outlet feeder Pipes). A jet of light water containing 6 cm<sup>3</sup> H<sub>2</sub>/kg H<sub>2</sub>O of dissolved hydrogen at a temperature of 310°C impinged on carbon steel disks. The pH was varied between 9.3 < pH<sub>25°C</sub> < 10.6. The results of the experiments are shown in Figure 2.4, expressed as terms of metal loss rate and oxide release rate. The rate of corrosion increases with increasing pH.

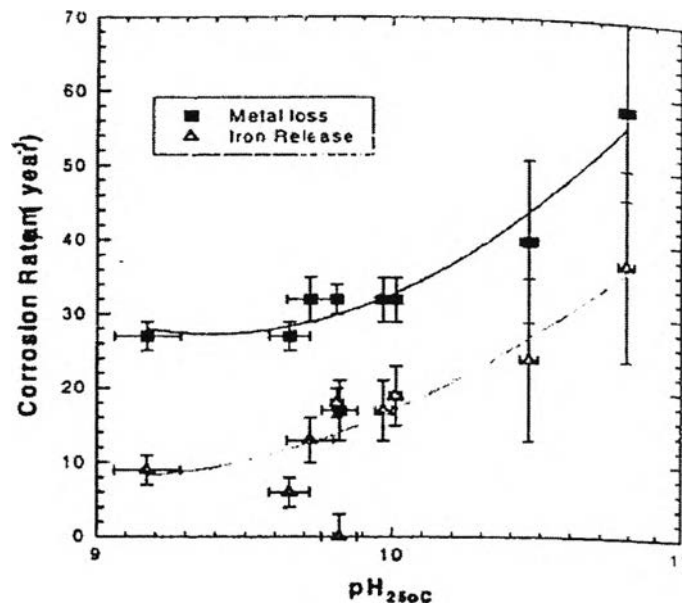


**Figure 2.4** Effect of pH on A106B corrosion rate (Lines show data trend).

The effect of pH on low carbon steel corrosion rates has also been investigated by Potter and Mann, 1962 as shown in Figure 2.5. The corrosion rate of steel is increased at 340°C by raising the concentration of sodium hydroxide. The qualitative reason for this seems plain: the inward diffusion of oxide ions through magnetite is accelerated by increasing the alkalinity, while the outward diffusion of iron ions is increased because more hydroxide ions are available to react with them at the outer surface of the magnetite.

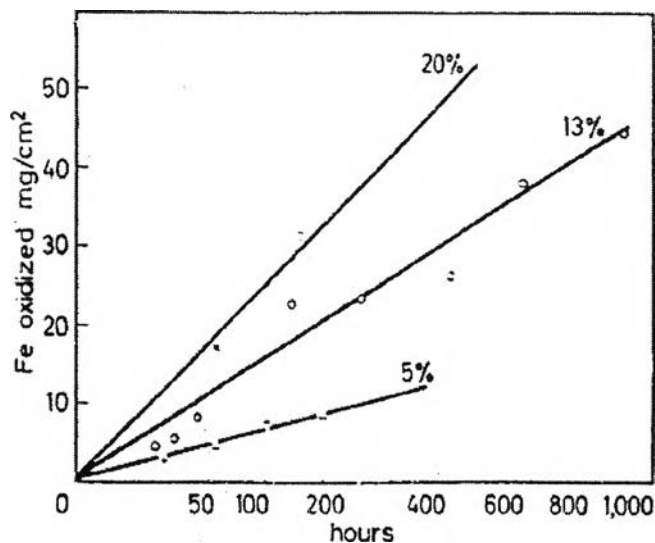


**Figure 2.5** Oxidation of mild steel at 340°C in aqueous sodium hydroxide at different percent by weight of sodium hydroxide (Plotted against square root time).

*Fluid velocity:*

As expected, metal loss increases with increasing flow velocity and turbulence. The effect of velocity on metal loss is determined by a complex interdependence among a number of parameters, including hydrodynamics, fluid chemistry, and metal oxide character.

Burrill and Cheluget (referenced in Corrosion of CANDU Outlet feeder Pipes) investigated the relationship between the minimum wall thickness in 2.5 inch diameter SA 106 Grade B carbon steel outlet feeder pipes after 12.3 Effective Full Power Years (EFPY) of operation with the average velocity in the range of 8.0-18.0 m/s, for CANDU 6 reactors. They found that data from 2.0 inch outlet feeder pipes indicate a similar trend. The fluid velocity significantly influences the wall rate loss. The angle of the first bend has a secondary influence, with thinning walls being observed with increasing bend angle. The average and maximum wall rate loss are proportional to the velocity raised to the power  $Z$ , i.e.  $\propto V^Z$ , where  $Z$  is larger than 1 and depends on pipe diameter and bend angle.



*Dissolved oxygen concentration:*

Bignold *et al.* (referenced in Erosion and Cavitation in the CANDU Primary Heat Transport System) showed that oxygen addition to achieve concentrations as low as 8 ppb in ammoniated water is beneficial in reducing FAC. This is a very important finding in that oxygen can effectively inhibit corrosion of carbon steel even when reducing agents (such as hydrazine or hydrogen) are present. These experiments have been performed up to a maximum temperature of 250°C.

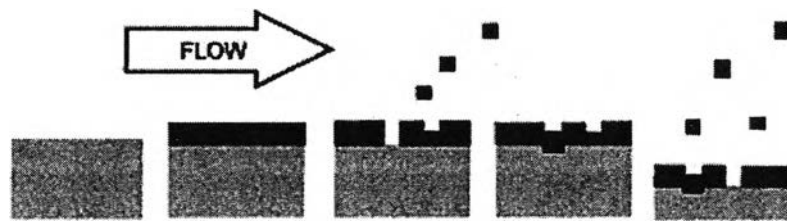


**Figure 2.6** Schematic of the mechanism for FAC (Marvin D. Silbert *et al.*, 2002).

FAC process, a magnetite oxide film forms on the carbon steel surface as a protective oxide layer due to the reaction between dissolved oxygen in flowing water or water/steam mixtures and the carbon steel surface. A protective oxide layer on a metal surface dissolves from the surface as dissolved iron, or forms a solid corrosion product which is mechanically swept from the metal surface and is carried downstream. A new oxide layer forms on exposed patches of the bare metal with continual removal and reforming of oxide, and thus the metal loss continues resulting in wall thinning as shown in Figure 2.6.

### 2.2.3 FAC in the Feeder Pipes in CANDU Reactors

The FAC effect can be investigated in the primary heat transfer system of the CANDU reactor. The outlet feeder pipes experience more FAC than inlet feeder pipes, since the coolant temperature rises from 265°C to 310°C during flow through the reactor core, where there is no source of iron, resulting in higher solubility of the oxide film for the outlet feeders. Therefore, the inlet feeder pipes

carry coolant saturated with dissolved iron, which results in a lower corrosion rate and a relatively thick oxide film compared with outlet feeder pipes.

### 2.3 Mechanism of Oxide Growth and Hydrogen Evolution

Magnetite ( $\text{Fe}_3\text{O}_4$ ) is the structure of iron oxide that is observed on a metal surface such as carbon steel in CANDU reactors. This type of oxide film behaves like a corrosion resistance film to the steel from the corrosive environment. The morphology of the oxide film is influenced by the chemical composition of the alloy, exposure conditions and surface finishing (Lister *et al.*, 1994).

Carbon steel corrodes in high temperature water and forms a double layer in supersaturated conditions, known as the Potter Mann layer. The inner layer consists of small magnetite crystals that grow into the metal, replacing the corroded volume (Potter and Mann, 1962). This layer grows at the metal-oxide interface and is compact and adherent (Potter and Mann, 1963) since it nucleates in the confined space. The outer layer consists of larger magnetite crystals since it grows by outward diffusion of the metal ions, especially iron, along oxide grain boundaries without volume constrain. The schematic of double oxide layer formed on carbon steel is shown in Figure 2.7.

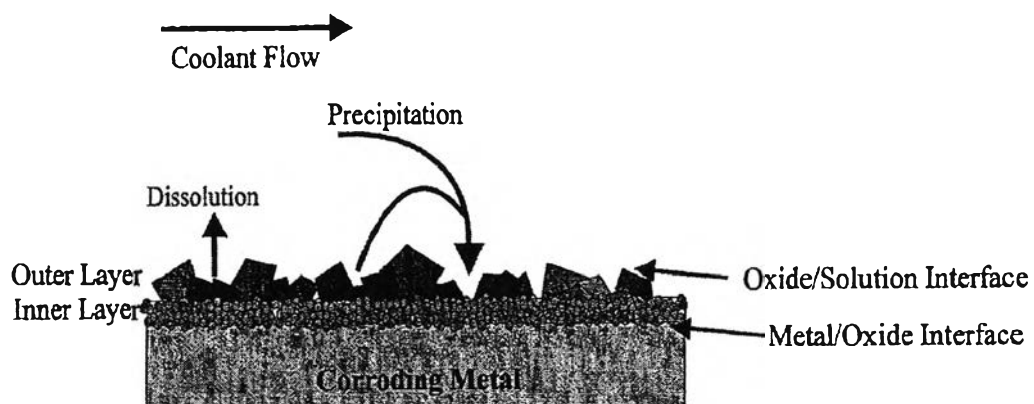
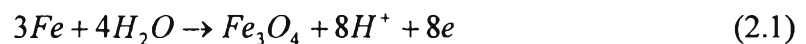


**Figure 2.7** Schematic of the double oxide layer formed on carbon steel (Lister *et al.*, 2001).

The corrosion of carbon steels and low alloy steels in high temperature water, in the absence of oxygen, involves the transport of oxygen-bearing species to the metal/oxide interface and outward movement of metal ions to the solution. When the solution becomes saturated with soluble iron, an outer magnetite layer is nucleated and grows on the surface. The net result is a double magnetite layer.

In the absence of oxygen, the inward movement of oxygen-bearing species occurs by diffusion either water molecules or oxygen ions or hydroxide ions. Since oxygen ions involve the formation of oxide film only after a sufficiently anodic potential is imposed and a de-protonation of water takes place, resulting in the loss of protons to the solution and oxygen ions migrating towards the steel surface. Therefore, oxygen ions cannot be the diffusion species. Since the oxide film thin, the electric charge strength across the film is high. The established electric field will block the negative charged ions, such as OH<sup>-</sup> from moving towards the steel surface. This eliminates hydroxide ions as the diffusion species. Therefore, the oxygen-bearing species involving the formation of the magnetite layer is probably water (Cheng and Steward, 2004).

A proposed schematic of the magnetite film formed on a steel surface in a high temperature water solution is shown in Figure. 2.8. Water molecules diffuse through the inner oxide layer and react directly with steel at the steel/oxide interface. Iron dissolution occurs where no oxide layer exists. Protons at the oxide/water interface diffuse through the oxide layer to consume the electrons produced by anodic reactions and discharge as hydrogen atoms at the steel/oxide interface. The relevant reactions occurring at the steel/oxide interface are:



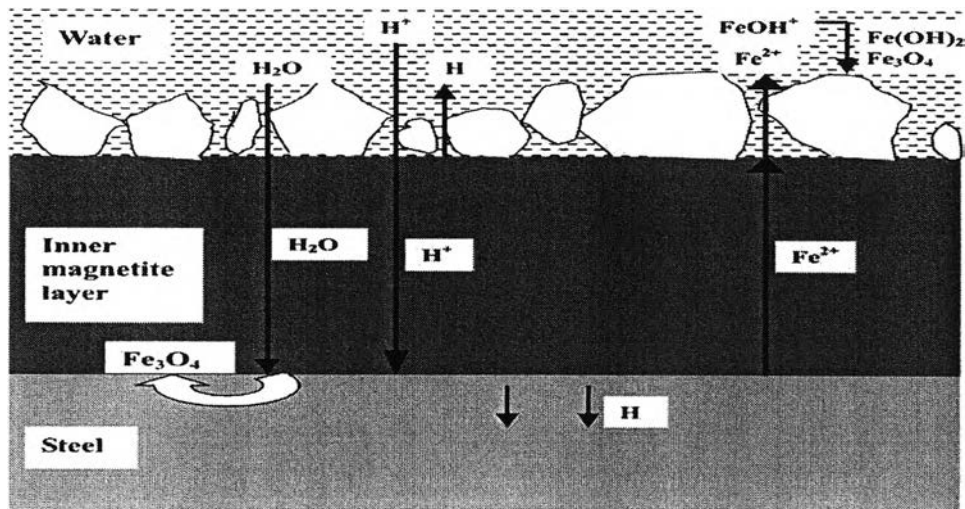
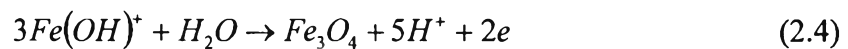


**Figure 2.8** Schematic of the formation mechanism of the magnetite film on the steel surface in high temperature water (Cheng and Steward, 2004).

The ferrous ions diffusing out of the oxide layer exist as  $\text{Fe}(\text{OH})^+$  in high temperature water must stabilize themselves by decreasing their charge/radius ratios through hydrolysis to form hydrous iron ions. The hydrous iron ions will deposit as loose  $\text{Fe}(\text{OH})_2$  once the saturation of the iron ion is achieved. The outer deposition of the magnetite layer is then formed in high temperature water, accompanying the discharge of hydrogen ions. Therefore, the electrochemical reactions occurring at the oxide/water interface are:



The reaction above indicates that hydrogen gas is produced by the carbon steel corrosion process.

Tomlinson (1981, 1989) studied the hydrogen emission during steel corrosion. He reported that protons produced from the corrosion process diffuse in both directions across the oxide, with the direction and magnitude of the proton flux being dependent on the structure of oxide layer. Hydrogen atoms are formed at both the metal/oxide interface and the oxide/water interface. At the oxide/water interface,

hydrogen atoms are either discharged at the oxide/water interface by electron diffusion across the oxide or diffusion through the oxide as protons which are discharged at metal/oxide interface. Under the concentration and potential gradient, protons at the oxide/water interface diffuse rapidly through the oxide layer and discharge as hydrogen atoms at the metal/oxide interface.

The experimental evidence indicates that up to 90% of the hydrogen atoms are generated at the metal/oxide interface during the corrosion of carbon steels by high temperature deaerated water. More than 99% of these hydrogen atoms will diffuse through the steel at the temperature of interest since it is generally accepted that the hydrogen diffusivity in an oxide film is very low. Hydrogen diffuses through the metal 330 times more quickly than through the oxide. It is suggested that if the rate of growth of the inner layer/ rate of growth of the outer layer is constant, then the ratio of hydrogen emission from metal and oxide surfaces should also be constant. Furthermore, the fraction of hydrogen passing through the steel appears to increase with the amount of oxide deposited on the tube surface.

## **2.4 The Fundamental Law of Diffusion**

### **2.4.1 Definition of Diffusion and Effusion**

Diffusion is the movement of a solute from an area of high concentration to an area of low concentration. Diffusion is a spontaneous process involving no fluid motion. The diffusivity of a substance is defined as the mass transferred per unit area per unit time in a fluid, under unit concentration gradient.

In solid diffusion mechanisms, vacancy diffusion and interstitial diffusion are the two most frequently encountered for the diffusion of atoms within solids. In vacancy diffusion, the transported atom jumps from a lattice position of the solid into a neighboring unoccupied lattice site or vacancy. The atom continues to diffuse through the solid by a series of jumps into other neighboring vacancies that appear to it from time to time. This normally requires a distortion of the lattice. An atom moves in interstitial diffusion by jumping from one interstitial site to a neighboring one. This normally involves a dilation or distortion of the lattice.

Moreover, in the crystal solid state, the occurrence of diffusion is upon the availability of point vacancies throughout the crystal lattice. Since the prevalence of point vacancies increases in accordance with the Arrhenius equation, the rate of crystal solid diffusion increases with temperature (Paul, 1963).

Effusion is the movement of a gas through a tiny opening or semi-permeable membrane into a lower pressure or vacuum. This occurs if the diameter of the hole is considerably smaller than the mean free path of the molecules. The rate at which gases effuse depends on their molecular weight; gases with a lower molecular weight effuse more rapidly than gases with a higher molecular weight. For two gases at the same temperature (and having the same specific heat), and thus having the same kinetic energy, the average molecular speed of each gas can be found using the equation  $E = (1/2)mv^2$ . Thus, lighter molecules have a higher speed. This results in more molecules passing through the hole per unit time.

#### 2.4.2 Fick's Law of Diffusion

Fick's Laws of diffusion describe mathematically the diffusion process.

##### 2.4.2.1 *Fick's First Law*

Fick's First Law is used for steady-state diffusion, i.e., when the concentration within the diffusion volume does not change with respect to time. In one dimension, this is given by:

$$J = -D \frac{\partial C}{\partial x} \quad , \quad (2.6)$$

where

$J$  is the diffusion flux in dimensions of [(amount of substance) length<sup>-2</sup> time<sup>-1</sup>], example  $\left(\frac{\text{mol}}{\text{m}^2 \cdot \text{s}}\right)$

$D$  is the diffusion coefficient or diffusivity in dimensions of [length<sup>2</sup> time<sup>-1</sup>], example  $\left(\frac{\text{m}^2}{\text{s}}\right)$

$C$  is the concentration of the diffusing substance in dimensions of

[(amount of substance) length<sup>-3</sup>], example  $\left(\frac{\text{mol}}{\text{m}^3}\right)$

$x$  is the coordinate chosen perpendicular to the reference surface in dimensions of [length], example ( $m$ )

The diffusion coefficient is proportional to the diffusing particles velocity, which is a function of the viscosity of the fluid, temperature, pressure and concentration. In steady state, Fick's First Law can be integrated to give

$$J = D \frac{(C_1 - C_2)}{l}, \quad (2.7)$$

where  $C_1$  and  $C_2$  are the concentration of penetrant at the feed and permeate sides, respectively, and  $l$  is the thickness of the diffusion path.

In two or more dimensions  $\nabla$ , the del or gradient operator generalizes the first derivative,

$$J = -D\nabla C \quad (2.8)$$

The driving force for the one-dimensional diffusion is the quantity  $\nabla C$  which is the concentration gradient.

#### 2.4.2.2 Fick's Second Law

Fick's Second Law is used for the non-steady or continually changing state diffusion, i.e., when the concentration within the diffusion volume changes with respect to time.

$$\frac{\partial C}{\partial t} = D \frac{\partial^2 C}{\partial x^2}, \quad (2.9)$$

where

$C$  is the concentration in dimensions of [(amount of substance) length<sup>-3</sup>], example [mol m<sup>-3</sup>]

$t$  is time in dimensions of [time], example [s]

$D$  is the diffusivity in dimensions of [length<sup>2</sup> time<sup>-1</sup>], example [m<sup>2</sup> s<sup>-1</sup>]

$x$  is the position in dimensions of [length], example [m]

It can be derived from the Fick's First Law and a mass balance:

$$\frac{\partial C}{\partial t} = -\frac{\partial J}{\partial x} = \frac{\partial}{\partial x} \left( D \frac{\partial C}{\partial x} \right) \quad (2.10)$$

Assuming the diffusivity (D) to be a constant one can exchange the orders of the differentiation, and multiplying by the constant:

$$\frac{\partial}{\partial x} \left( D \frac{\partial C}{\partial x} \right) = D \frac{\partial}{\partial x} \frac{\partial C}{\partial x} = D \frac{\partial^2 C}{\partial x^2} \quad (2.11)$$

This obtains the form of Fick's equations as stated above.

For the case of diffusion in two or more dimensions the Second Fick's Law is:

$$\frac{\partial C}{\partial t} = D \nabla^2 C \quad , \quad (2.12)$$

which is analogous to the heat conduction equations given by Fourier's Law.

If the diffusivity is not a constant, but depends upon the coordinate and/or concentration, the Second Fick's Law becomes:

$$\frac{\partial C}{\partial t} = \nabla \cdot (D \nabla C) \quad (2.13)$$

An important example is the case where C is at a steady state, i.e. the concentration does not change with time, so that the left part of the above equation is identically zero. In one dimension with constant diffusivity (D), the solution for the concentration will be a linear change of concentrations along x. In two or more dimensions one obtains:

$$\nabla^2 C = 0 \quad , \quad (2.14)$$

which is Laplace's equation, the solutions to which are called harmonic functions by mathematicians.



### 2.4.3 Sievert's Law

Hydrogen permeation through membranes has been modeled using the solution-diffusion approach, in which the hydrogen molecules dissociatively adsorb on the metal surface, adsorb into and diffuse through the bulk in atomic H form, and recombine and desorb as molecular hydrogen at the permeate side. When diffusion of hydrogen atoms through the bulk metal is the rate limiting step and there are no surface effects on both sides of specimen, hydrogen permeation flux is at steady state,  $J$  (mol/m<sup>2</sup> s), and can be described by Sievert's Law:

$$J = \frac{Q}{l} \left( \sqrt{P_{H_2,f}} - \sqrt{P_{H_2,p}} \right) , \quad (2.15)$$

where  $Q$  is the permeability of hydrogen through the membrane (mol/m s Pa<sup>0.5</sup>),  $l$  is the membrane thickness (m), and  $P_{H_2,f}$  and  $P_{H_2,p}$  are the feed and permeate side partial pressures of hydrogen, respectively. The derivation of Sievert's Law also assumes that the surface coverage of hydrogen at both the feed and permeate sides of the membrane is in equilibrium with the respective fluid phases, and that the adsorption equilibrium constant is the same on both sides:

$$C = K P_{H_2}^{0.5} , \quad (2.16)$$

where  $C$  is the atomic hydrogen concentration on the membrane surface,  $K$  is the dissociative adsorption equilibrium constant and  $P_{H_2}$  is the hydrogen partial pressure. The 0.5 exponent comes from dissociative adsorption of a diatomic molecule and gives the square root of hydrogen pressures in the flux equation above.

From the numerous measurements of Sieverts and others, it proves that the solubility of gases having diatomic molecules is proportional to the square of the hydrogen gas pressure. According to Henry's law, if the molecular condition of the hydrogen gas in the metal is the same as in the gaseous state the solubility should be proportional to the hydrogen pressure, which may be expressed by the equation

$$P_{H_2} = k C_{H_2} , \quad (2.17)$$

where

$P_{H_2}$  is the pressure of the hydrogen gas

$C_{H_2}$  is the concentration of molecular hydrogen in the metal

On the other hand if the hydrogen gas in solution can be assumed to be dissociated, the equilibrium between atomic and molecular hydrogen in the metal is then expressed by the equation

$$C_{H_2} = k_1(C_H)^2 \quad (2.18)$$

And from equation (2.17)

$$P_{H_2} = kC_{H_2} = kk_1(C_H)^2 \quad (2.19)$$

or

$$C_H = k_2\sqrt{P_{H_2}} \quad (2.20)$$

The solubility would, therefore, be proportional to the square root of the pressure. Since the rate of diffusion will depend on the concentration of gas in the metal it may be expected that diffusion will be proportional to the square root of the gas pressure which is in agreement with the experimental results as shown in Figure 2.9 for hydrogen/iron system.

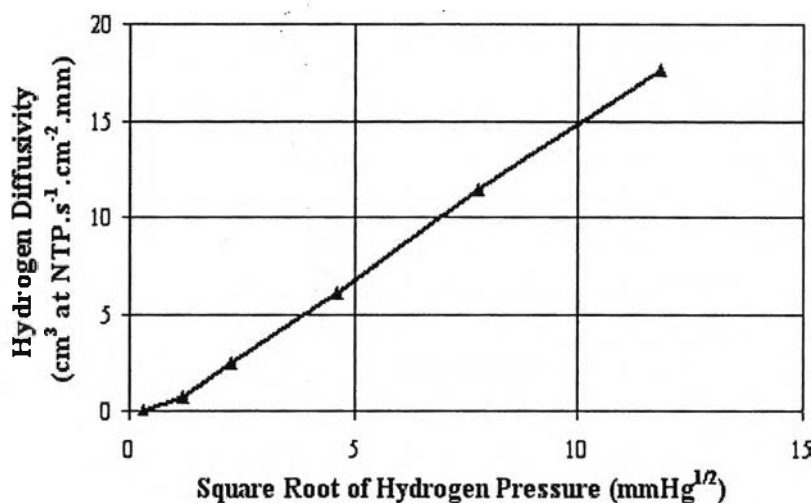


**Figure 2.9** Diffusion of hydrogen through iron (etched surface): the rate of diffusion (D) is expressed as the volume of gas in cubic centimeters at N.T.P. diffusing per second through 1 sq cm of surface of 1 mm thickness (Smithells and Ransley, 1935).

Sievert's Law is widely applied in analyzing hydrogen permeation through membranes, even in some cases where the assumptions made in deriving Sievert's Law are not valid.

#### 2.4.4 Graham's Law of Effusion

Graham's law of effusion was formulated by Thomas Graham. Graham found experimentally that the rate of effusion of a gas through a porous metal is inversely proportional to the square root of the mass of its particles. This formula can be written as:

$$\frac{Rate_1}{Rate_2} = \sqrt{\frac{M_2}{M_1}}, \quad (2.21)$$

where

$Rate_1$  is the rate of effusion of the first gas

$Rate_2$  is the rate of effusion of the second gas

$M_1$  is the molar mass of gas 1

$M_2$  is the molar mass of gas 2

Graham's Law states that the rate of diffusion of a gas is inversely proportional to the square root of its molecular weight. Thus, if the molecular weight of one gas is four times that of another, it would diffuse through a porous plug or escape through a small pinhole in a vessel at half the rate of the other.

Graham's Law is most accurate for molecular effusion which involves the movement of one gas at a time through a hole. It is only approximate for diffusion of one gas in another or in air, as these processes involve the movement of more than one gas.

Graham's Law can also be used to find the approximate molecular weight of a gas if one gas is a known species, and if there is a specific ratio between the rates of two gases. The equation can be solved for either one of the molecular weights provided the subscripts are consistent.

$$M_2 = \frac{M_1(\text{Rate}_1)^2}{(\text{Rate}_2)^2} \quad (2.22)$$

#### 2.4.5 Arrhenius Equation

The Arrhenius equation is an expression for the temperature dependence of the rate constant of chemical reactions on the absolute temperature and activation energy. In the case of the diffusion coefficient ( $D$ ) at difference temperatures, Arrhenius's Law is often found to give a good prediction of the variation of the diffusion coefficient with temperature as shown in Equation 2.23

$$D = D_0 \cdot e^{\frac{-E_A}{RT}}, \quad (2.23)$$

where

$D$  is the diffusion coefficient in dimensions of  $[\text{length}^2 \cdot \text{time}^{-1}]$

$D_0$  is the maximum diffusion coefficient (at infinite temperature) in dimensions of  $[\text{length}^2 \cdot \text{time}^{-1}]$

$E_A$  is the activation energy for diffusion in dimensions of  $[\text{energy} (\text{amount of substance})^{-1}]$

$T$  is the absolute temperature in dimensions of  $[\text{absolute temperature}]$

$R$  is the gas constant in dimensions of  $[\text{energy temperature}^{-1} (\text{amount of substance})^{-1}]$

The maximum diffusion coefficient ( $D_0$ ) can be obtained from a plot of natural log of  $D$  vs.  $1/T$ , called an Arrhenius plot. The slope gives the activation energy for diffusion ( $E_A$ ) and the projection to infinite ( $1/T \rightarrow 0$ ) gives  $\ln D_0$ .

Solubility ( $S$ ) and permeability ( $P$ ) are temperature dependent like the diffusivity and can be represented by an Arrhenius equation as followed.

$$S = S_0 \exp\left(\frac{-E_S}{RT}\right) \quad (2.24)$$

$$P = P_0 \exp\left(\frac{-E_p}{RT}\right) \quad (2.25)$$

where  $P = SD$  (2.26)

## 2.5 Diffusion Coefficient of Hydrogen in Metal

### 2.5.1 Mechanism of Hydrogen Transport Through Metal

Hydrogen permeation in metals and alloys is a complicated phenomenon including several successive stages: adsorption of the molecule upon the surface, dissociation into adsorbed atoms, diffusion of the adsorbed atoms, recombination into molecule and desorption. It is often assumed that the surface processes play an insignificant role in the gas permeation through metals and alloys since it is considered that they are much faster than the diffusion itself (Addach *et al.*, 2005).

In addition to its diffusion through the bulk metal, the permeation of hydrogen through steels involves its entrance at one surface and its exit at the other surface of the specimen. There are seven steps that take place before the hydrogen is detected on the output side of the specimen. Figure 2.10 shows the seven steps that take place in the permeation of hydrogen through a metallic membrane.

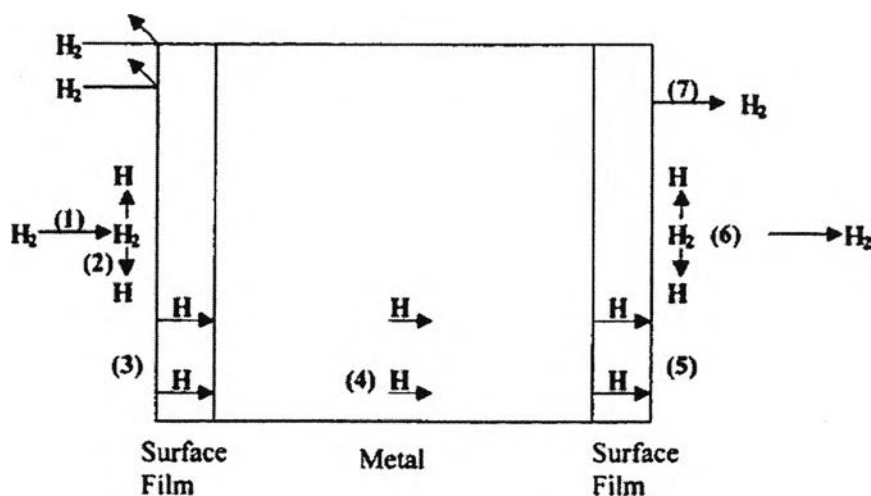


**Figure 2.10** Seven steps of hydrogen permeation (Stone, 1981).

This model takes into account the presence of surface films on both input and output sides of the specimen. The seven steps are:

1. Adsorption of hydrogen molecule on the surface.
2. Dissociation of the adsorbed molecule on the surface.
3. Permeation of dissociated atoms through the surface film (oxide).
4. Permeation of atoms through the metal.
5. Permeation of atoms through the film on the output side.
6. Reassociation of atoms to form H<sub>2</sub> molecule.
7. Desorption of the reassociated H<sub>2</sub> molecule.

In the case of corrosion in feeder pipes in CANDU reactors, hydrogen is produced as hydrogen atoms as a consequence of flow-accelerated corrosion (FAC). Therefore hydrogen is present at the metal surface as atomic hydrogen which directly adsorbs and diffuses through the metal, the dissociation step is avoided.

## 2.5.2 Hydrogen Diffusivity Determination Methods

For the determination of hydrogen diffusivity, the following five methods are generally used (Janusz Flis, 1991).

### 2.5.2.1 *State-State Flow Method*

In the steady-state flow method which allows the calculation of hydrogen diffusivity from the experimental values of the steady-state rates of hydrogen permeation through a metal layer, provided that the solubility or concentration of the gas in the material studied is known under the conditions of the experiment, from the equation:

$$P_{\infty} = \frac{Dc}{l} \quad , \quad (2.27)$$

where

$P_{\infty}$  is the hydrogen permeation rate at steady-state

$D$  is the hydrogen diffusivity in the material examined

$c$  is the concentration of the dissolves

(also called diffusible or lattice) hydrogen

$l$  is the material examined thickness

### 2.5.2.2 Hydrogen Absorption or Desorption Method

Measurements of hydrogen absorption or desorption rates are used for the determination of hydrogen diffusivity, particularly at high temperature. Solutions of the diffusion equations under suitable initial and boundary conditions yield simple formulae for the determination of hydrogen diffusivity.

### 2.5.2.3 Time Lag Method

The classical time lag method is derived from Fick's second law and has been widely used. The time lag method ignores the absorption and desorption processes (Addach *et al.*, 2005). This method consists of measuring the quantity of gas which diffuse through a metal layer of a known thickness in time  $t$  and determining from this the time lag  $t_L$ . The diffusivity of hydrogen is estimated from the formula,  $D = l^2/6t_L$ . If the hydrogen permeation rate is measured as a function of time, i.e.  $P = f(t)$ , the time lag  $t_L$  then equals the time after which  $P = 0.63P_\infty$ .

### 2.5.2.4 Electrochemical Method

Application of the electrochemical method for the measurement of hydrogen permeation rate has allowed the development of a number of new techniques for the determination of diffusivity of hydrogen. One of these is the method of standardized curves of the absorption and desorption of the hydrogen permeation rate with time which occur after the cathodic polarization current is switched on and off respectively. In this method, hydrogen diffusivity is found from relation  $\tau = Dt/l^2$ . An advantage of this method is that hydrogen diffusivity can be evaluated for various concentrations of the diffusing gas from a single experimental curve of the absorption or desorption of the hydrogen permeation rate with time.

### 2.5.2.5 Internal friction Method

This method is based on the view that the diffusivity value for hydrogen at low temperatures can be found from a study of the internal friction of hydrogen-charged iron specimens as a function of temperature.

### 2.5.3 Hydrogen Diffusivity in Iron

The diffusion coefficient ( $D$ ) is dependent on temperature, pressure and composition of the system. Diffusion coefficients are generally higher for gases (in the range of  $5 \times 10^{-6}$  to  $1 \times 10^{-5}$   $\text{m}^2/\text{s}$ ) than for liquids (in the range of  $10^{-10}$  to  $10^{-9}$   $\text{m}^2/\text{s}$ ) which are higher than the values reported for solids (in the range of  $10^{-14}$  to  $10^{-10}$   $\text{m}^2/\text{s}$ ) (Welty, 2001).

The diffusion of hydrogen in iron has been widely discussed in several reviews in terms of the dependence of diffusivity of hydrogen on temperature or Arrhenius equation;  $D = D_0 \exp\left(-\frac{E}{RT}\right)$ . The values of the diffusion coefficient of hydrogen obtained by many investigators are shown in Figures 2.11 and 2.12.

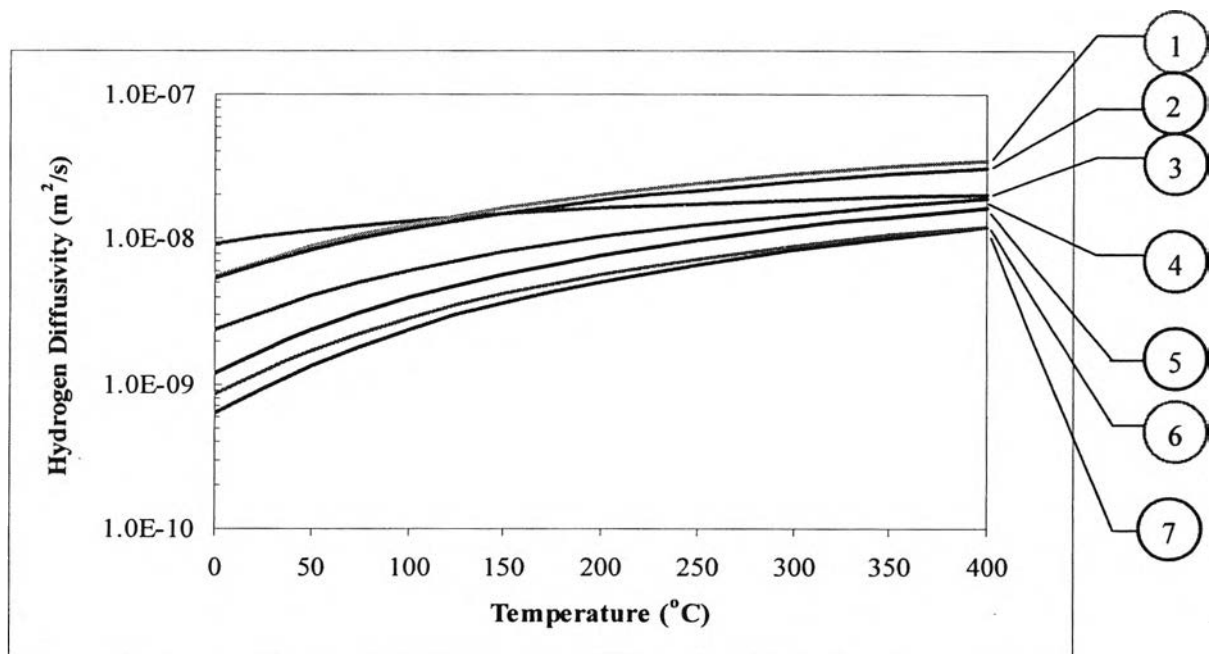


**Figure 2.11** Diffusion coefficients of hydrogen through iron.



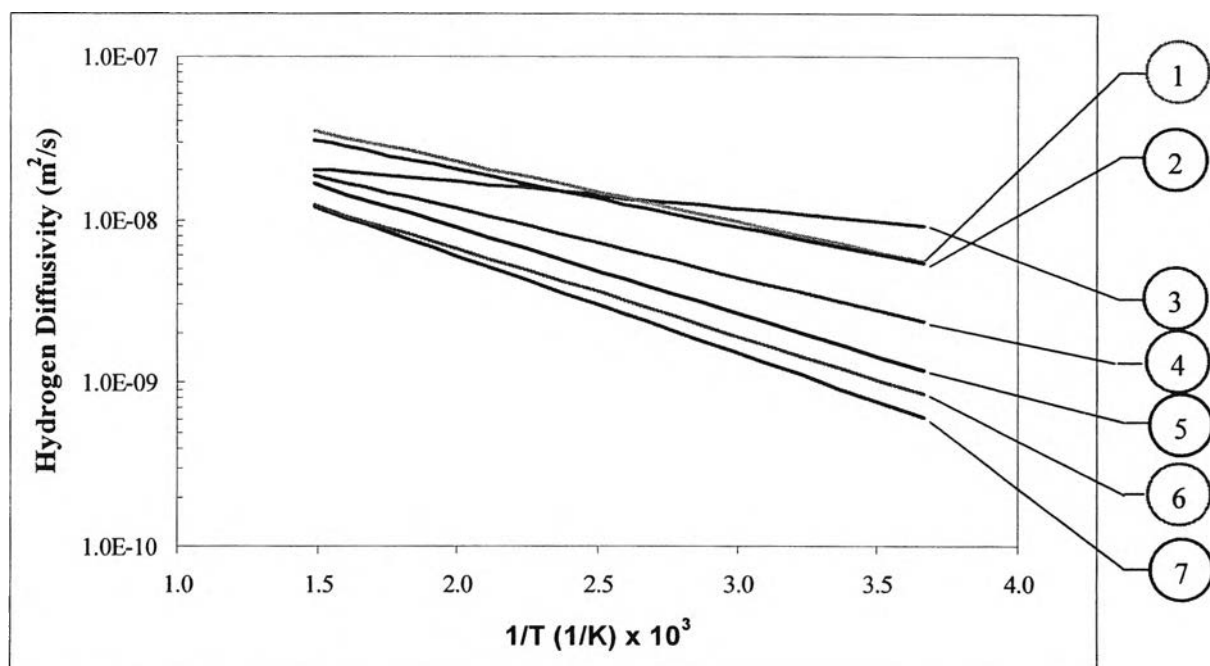


**Figure 2.12** Hydrogen diffusivity in iron vs. reciprocal absolute temperature on the basis of various data: 1-from Equation (2.28), 2-from Equation (2.29), 3-from Equation (2.30), 4-from Equation (2.31), 5-from Equation (2.32), 6-from Equation (2.33) and 7-from Equation (2.34).

Flis, 1991 “Corrosion of Metals and Hydrogen-Related Phenomena”:

$$D = 1.23 \times 10^{-7} \exp\left(\frac{-847.97}{T}\right) \quad (2.28)$$

Miller *et al.*, 1975 “Permeation of Hydrogen Through Alpha Iron”:

$$D = 1.01 \times 10^{-7} \exp\left(\frac{-802.72}{T}\right) \quad (2.29)$$

Flis, 1991 “Corrosion of Metals and Hydrogen-Related Phenomena”:

$$D = 3.57 \times 10^{-8} \exp\left(\frac{-372.87}{T}\right) \quad (2.30)$$

Flis, 1991 “Corrosion of Metals and Hydrogen-Related Phenomena”:

$$D = 7.8 \times 10^{-8} \exp\left(\frac{-956.22}{T}\right) \quad (2.31)$$

Flis, 1991 “Corrosion of Metals and Hydrogen-Related Phenomena”:

$$D = 9.85 \times 10^{-8} \exp\left(\frac{-1,202.79}{T}\right) \quad (2.32)$$

Alefeld and Völkl, 1978 “Hydrogen in metal I”:

$$D = 7.5 \times 10^{-8} \exp\left(\frac{-1,218.81}{T}\right) \quad (2.33)$$

Salii *et al.*, 1973 “Permeation, Diffusion, and Solubility of Hydrogen in Pure Alpha Iron”:

$$D = 9 \times 10^{-8} \exp\left(\frac{-1,358.83}{T}\right) \quad (2.34)$$

The diffusion coefficient of hydrogen dependence on temperature reported by Equation 2.28 to 2.34 shows a slight discrepancy. The hydrogen diffusivity differ one order of magnitude at high temperature. The reasons for this are diverse and it is not always easy to determine which one is the major factor. Among the possible reasons for variations are: surface processes, interaction of hydrogen with linear defects, and the development of micro-cracks and blisters in metal as induced by hydrogen. Another possible reason for this is that reliable measurement of hydrogen solubility in iron can only be made at temperatures above approximate 573 K. This is due to a low solubility of this gas in iron at lower temperatures (Flis, 1991). In addition, the rate of hydrogen entry into the metal is much influenced by many variables such as its composition, thermal-mechanical history, presence of surface layer, presence of impurity, diffusion measuring method, pressure range of measurement etc. (Matei, 1999).

Hydrogen traps may be caused by various defects in the crystal structure of the metal such as dislocations, inclusions boundaries, voids and micro-cracks etc. Booth *et al.*, 1975 advanced a model for the diffusion of hydrogen in iron and steel containing hydrogen traps in the form of voids. They assumed firstly that hydrogen in iron alloys occurs in two forms, either dissolved in the crystal lattice of the metal, or molecular hydrogen present in voids, and secondly that an equilibrium exists between these two forms. For a quantitative description of the dependence of dissolved hydrogen concentration on the equilibrium pressure of molecular hydrogen in voids, Phragmen's equation was used. The solution of this equation for various cases shown that at room temperature, increased volume concentration of voids from zero to  $10^{-14}$  lowers the value of the hydrogen diffusivity by about two orders of magnitude.

McNabb and Foster (1963) demonstrated theoretically that in the case of diffusion of hydrogen through metal membranes containing hydrogen traps, the time lag is a function of not only the number of hydrogen traps but that it also depends on membrane thickness, concentration of diffusible hydrogen and the kinetic parameters of the processes of the hydrogen trapping and releasing.

Owczarek and Zakroczymski (2000) performed an experiment to confirm the effect of the membrane thickness used on the hydrogen transport in a duplex stainless steel by the electrochemical technique. The results shown that the apparent coefficients of hydrogen diffusion in a duplex stainless steel decrease with the membrane thickness. Moreover the hydrogen diffusivity also depended on a kind of permeation curve (first build up, partial decay or build up, or complete decay transients) and a base of analysis (characteristic points of the permeation curve or the entire curve) as shown in Figure 2.13.

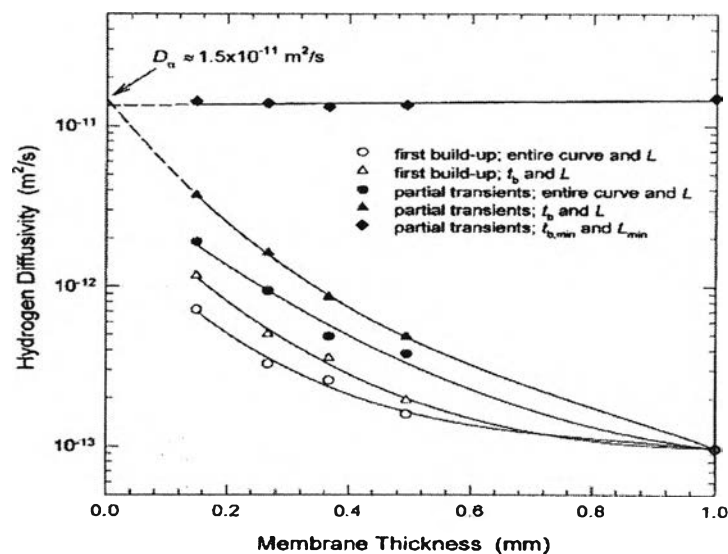


**Figure 2.13** Hydrogen diffusivity evaluated by different procedures as a function of the membrane thickness.

Carbon is always used to strengthen steel. For carbon steel, adding carbon in iron leads to a decrease of the hydrogen diffusion coefficient and hydrogen permeability. In case of additions of 1%wt carbon to Fe-16Al wt%, the results show a decrease in hydrogen permeability and diffusivity by a factor of 2. However, the hydrogen solubility in the alloy does not change with carbon addition (Parvathavarthini *et al.*, 2002). An increase in carbon content from 0.045 to 0.085% has been reported to lead a decrease in the diffusion coefficient of hydrogen by a factor of 8 in 304 stainless steel. Apparently, the carbides in the steel lower the diffusional mobility of hydrogen.

#### 2.5.4 Hydrogen Diffusivity in Oxide Films

Thin oxide films (90-1000Å) of an  $\alpha$ -Fe<sub>2</sub>O<sub>3</sub> type structure on 302 and 307 stainless steel have been shown to be a substantial barrier to hydrogen diffusion. The diffusion coefficients of the oxide films are in the range of  $1.8 - 66 \times 10^{-21} \text{ m}^2/\text{s}$  while the diffusion coefficient of stainless steel is about  $10^{-12} \text{ m}^2/\text{s}$ . The value of the diffusion coefficient for the oxides depends on its chemical composition: films of  $\alpha$ -Fe<sub>2</sub>O<sub>3</sub> (formed on pure iron) had a diffusion coefficient of  $0.1 \times 10^{-21} \text{ m}^2/\text{s}$ , and films of Cr<sub>2</sub>O<sub>3</sub> (formed on pure chromium) had a diffusion coefficient of  $92 \times 10^{-21} \text{ m}^2/\text{s}$ . In addition, the hydrogen diffusivity also depends on the oxide thickness due to changes in chemical composition of the oxide with thickness. The effectiveness of the oxide film as a barrier against hydrogen diffusion was lost when the film thickness exceeded about 1000Å, probably due to cracking. The changing of the crystal size of the substrate and oxide had no effect on the hydrogen diffusion rate (Piggott and Siarkowski, 1972).

Schomberg and Jürgen Grabke (1996) studied the hydrogen permeation in the passive film formed on the exit side of the iron membrane by chemical polishing using the sensitive electrochemical technique. The iron surface on the entry side was palladium coated to make a clean and oxide-free surface which is required for unretarded hydrogen uptake. The results indicated that the oxide film is nearly impermeable for hydrogen, even if the hydrogen is in the atomic or protonic state. They suggested that if the oxide films were situated on the hydrogen entry side, the surface reaction or hydrogen dissociation would be strongly retarded and hydrogen uptake would not be possible. On the other hand, hydrogen uptake and permeation of the oxide film may be possible if the hydrogen arriving at the iron/oxide interface is in an atomic/protonic state by coating the surface with palladium.

The measured permeation coefficients describe both the permeation through the iron membrane and the permeation through the thin oxide film. The hydrogen permeation coefficients for the film itself could be calculated assuming that the reciprocal of the permeation coefficient related to layer thickness behaves as a

permeation resistance in series. (Schomberg *et al.*, 1994 and Schomberg and Grabke, 1996). The following equation is obtained from Ohm's and Kirchhoff's law:

$$\frac{d_{Fe/oxide}}{\Phi_H^{Fe/oxide}} = \frac{d_{Fe}}{\Phi_H^{Fe}} + \frac{d_{oxide}}{\Phi_H^{oxide}}, \quad (2.35)$$

where

$d$  is the thickness of each layer

$\Phi$  is the permeation coefficient in each layer

This leads to an expression for the permeation coefficient of the oxide, respectively oxide layer:

$$\Phi_H^{oxide} = \frac{d_{oxide}}{\frac{d_{Fe/oxide}}{\Phi_H^{Fe/oxide}} - \frac{d_{Fe}}{\Phi_H^{Fe}}} \quad (2.36)$$

### 2.5.5 Hydrogen Diffusivity in Iron Alloys

Hydrogen diffusion in steels and its alloy is complicated because of the complex microstructure. Many works, however, have been reported on the hydrogen diffusivity through the membranes of iron alloys.

#### 2.5.5.1 *Fe-Ni Alloy*

Nickel is added to iron to improve its properties because of its resistance to many corrosives. Nickel forms a good base for alloys requiring strength at high temperatures. For example, 2% nickel cast iron is much superior to unalloyed cast iron. Another important attribute is the large and rapid increase in stress-corrosion resistance as the nickel content of stainless alloys increase above 10%.

Robertson (1977) studied the hydrogen diffusion in two high strength superalloys, Inconel 718 and Incoloy 903. Measurements were made over the temperature range of 150 to 500 °C, with applied hydrogen pressures of 1 to 3 atm. The author indicated that the temperature dependence of the hydrogen diffusion coefficient for Inconel 718 and Incoloy 903 can be described by the equations,

$$D_{Inconel718} = 1.07 \times 10^{-6} \exp\left(\frac{-11,900}{RT}\right) \frac{m^2}{s}, \quad (2.37)$$

$$D_{Incoloy903} = 2.46 \times 10^{-6} \exp\left(\frac{-12,590}{RT}\right) \frac{m^2}{s}, \quad (2.38)$$

where the activation energies are in cal/mole.

#### 2.5.5.2 Fe-Cr Alloy

An increase in chromium content can reduce the corrosion rate of steel at high temperature due to the higher packing density and smaller particle sizes of the oxide layer (Taenumtrakul, 2005). In metallurgy, an iron-carbon alloy with a minimum of 11% chromium is defined as stainless steel (Fontana, 1986). Chromium is a reactive element, but it and its alloy passivate and exhibit excellent resistance to many environments that makes it an ideal base material for many commercial applications.

Balasubramaniam and Kumar (1997) performed experiments to determine the hydrogen diffusivity in three austenitic stainless steels (304, 310 and 316) by subscale microhardness profiling after cathodic hydrogen charging. The hydrogen diffusivity was estimated using the standard diffusivity equation. The estimated diffusivity of hydrogen at 304K in 304, 310 and 316 stainless steels are  $2.86 \times 10^{-13}$ ,  $1.16 \times 10^{-13}$  and  $1.78 \times 10^{-13}$  m<sup>2</sup>/s, respectively. This is in good agreement with the reported diffusivity of hydrogen in Fe-Cr and Fe-Ni steels at room temperature. The hydrogen diffusivity at room temperature does not depend on the composition of austenitic stainless steels, in conformity with the behavior of hydrogen and its isotopes in austenitic stainless steels at high temperature.

Zakroczymski *et al.* (2002) performed experiments to study hydrogen adsorption in a duplex stainless steel by the electrochemical technique. The obtained permeation and desorption rates were analyzed in the ferrite phase. They found that the value of the hydrogen diffusivity is  $1.5 \times 10^{-11}$  m<sup>2</sup>/s at room temperature which is 480 times lower than the diffusivity of hydrogen in pure iron ( $7.2 \times 10^{-9}$  m<sup>2</sup>/s). In addition, the hydrogen content in each phase of the steel is different. The hydrogen content is  $1.6 \times 10^{-6}$  and  $27.8 \times 10^{-6}$  mol H/cm<sup>2</sup> for diffusible hydrogen (ferrite phase) and trapped hydrogen (austenite phase), respectively.

### 2.5.6 Hydrogen Diffusivity in Carbon Steel

Carbon steel is alloyed, singly or in combination, with chromium, nickel, copper, molybdenum, phosphorous and vanadium in the range of a few percent or less to produce low-alloy steels. The higher alloy additions are usually for better mechanical properties and hardenability. The lower range of about 2% total maximum is of greater interest from the corrosion standpoint. Strengths are appreciable higher than carbon steel, but the most important attribute is much better resistance to atmospheric corrosion.

Yuan (2007) investigated hydrogen permeation behavior in ultra-low carbon steel. It was found that the diffusion coefficient of hydrogen in ultra-low carbon steel annealed at 730 °C for 5 h. and annealed at 870°C for 6 min is  $9.57 \times 10^{-11}$  and  $1.4 \times 10^{-10}$  m<sup>2</sup>/s at 25°C, respectively.

Ichitani *et al.* (2003) investigated the visualization of hydrogen diffusion in steels by both a high sensitivity hydrogen microprint technique (HMT) and an electrochemical hydrogen permeation method. The permeation rate of hydrogen through extremely low carbon steel and hypo-eutectoid steel are  $8.2 \times 10^{-7}$  and  $7.7 \times 10^{-7}$  mol/m<sup>2</sup>s, respectively. The diffusion coefficient of hydrogen in hypo-eutectoid steel is about half that in low carbon steel. The diffusion coefficient of hydrogen in extremely low carbon steel is  $1.1 \times 10^{-9}$  m<sup>2</sup>/s while the diffusion coefficient of hydrogen in hypo-eutectoid steel is  $5.4 \times 10^{-10}$  m<sup>2</sup>/s. These results agree with the general rule that the diffusion coefficient decreases with increasing carbon content in steels.

In 2006 Hiller and Robinson performed hydrogen permeation measurements to study hydrogen uptake by steel electroplated with alloys using a modification of the two-cell permeation technique. They found that the hydrogen diffusivity in a low carbon steel membrane is  $3.8 \times 10^{-12}$  m<sup>2</sup>/s at 50°C. The hydrogen diffusivity for nickel is very low, of the order of  $8 \times 10^{-14}$  m<sup>2</sup>/s compared to  $2.5 \times 10^{-11}$  m<sup>2</sup>/s for high strength steel. The presence of even a very thin layer of nickel at the metal/coating interface would act as an effective barrier to hydrogen uptake.



### 2.5.7 Hydrogen Diffusivity in Palladium

Völkl and Alefeld (1978) collected the temperature dependence of the diffusion coefficient data from many authors and used the Arrhenius equation to approximate the maximum diffusion coefficient (at infinite temperature) and the activation energy of diffusion for palladium.

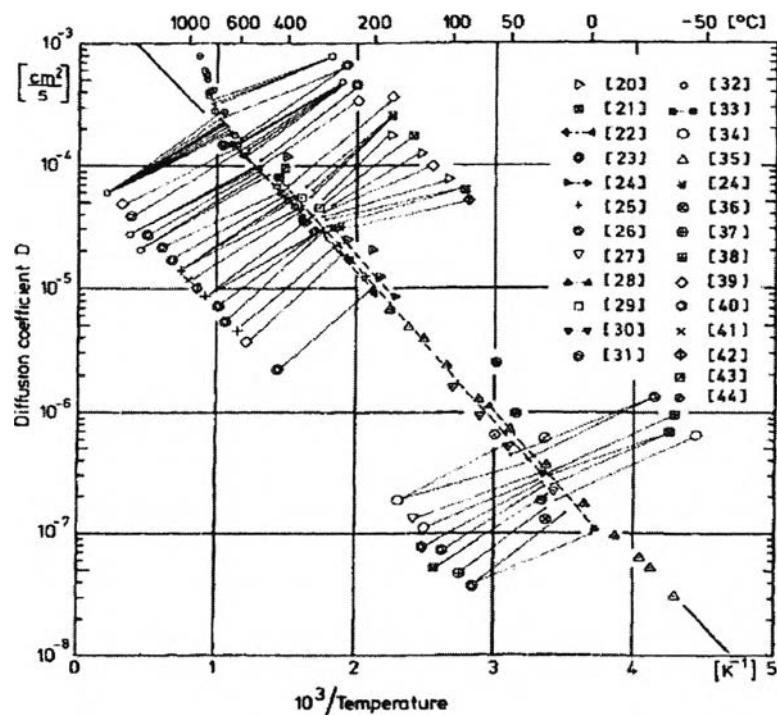


**Figure 2.14** Diffusion coefficient of hydrogen in palladium (Number in brackets refer to references of diffusion of hydrogen in metals, Hydrogen in metals I).

It appears that the maximum diffusion coefficient and the activation energy of diffusion of palladium are  $2.9 \times 10^{-7} \text{ m}^2/\text{s}$  and  $22,196.47 \text{ J/mol}$ , respectively as shown in Equation (2.39).

$$D = 2.9 \times 10^{-7} \exp\left(\frac{22,196.47}{RT}\right), \quad (2.39)$$

where  $R$  is  $8.314 \text{ J/mol.K}$  and  $T$  is the absolute temperature (K).

### 2.5.8 Hydrogen Diffusivity in Copper

The diffusivity of hydrogen in copper at low temperatures using electrochemical method was studied by Ishikawa and Mclellan (1985). The hydrogen diffusivity in copper was measured in the temperature range 299-322.5K. The data at high temperature from other investigators were subjected to a least-squares regression, and the resulting best-fit line is given by

$$D = 2.11 \times 10^{-6} \exp\left(\frac{-44,530}{RT}\right) \frac{m^2}{s}, \quad (2.40)$$

where  $R = 8.314 \text{ J/mol.K}$ . This hydrogen diffusivity is extrapolated to low temperatures that pass through the current results in this experiment and there are no deviations from classical Arrhenius diffusion behavior in the entire temperature range from 1200 down to 300K. Another determination of the dependence of diffusivity of hydrogen in copper on temperature at low temperature was determined by Sakamoto and Takao (1982) who used the electrochemical permeation method, as shown in Equation (2.41).

$$D = 3.69 \times 10^{-7} \exp\left(\frac{-36,820}{RT}\right) \frac{m^2}{s}, \quad (2.41)$$

where  $R = 8.314 \text{ J/mol.K}$ .

## 2.6 Effects of Isotope Dependence and Structure of Metal

Deviations from the predictions of classical rate theory  $D_1/D_2 = \sqrt{m_2/m_1}$  have been observed for all metal-hydrogen systems. This is not too unexpected in the light of the small masses and the high Einstein temperatures of the hydrogen isotopes. The characteristic features of the isotope dependence seem to be correlated with the structure of the host metal as discussed by several investigators. For the three bcc metals; hydrogen diffuse through Vanadium, Niobium and Tantalum was faster than deuterium in the temperature region investigated. The pre-exponentials are almost isotope independent whereas for the activation energies of hydrogen are lower than that of deuterium. As a consequence, the ratio of  $D_H/D_D$  shown in Figure 2.15 for the three metals is temperature dependent. Only at a definite temperature which is

about the same for all three metals is this ratio  $\sqrt{2}$ , whereas at lower temperatures, ratios up to about 20 have been observed.

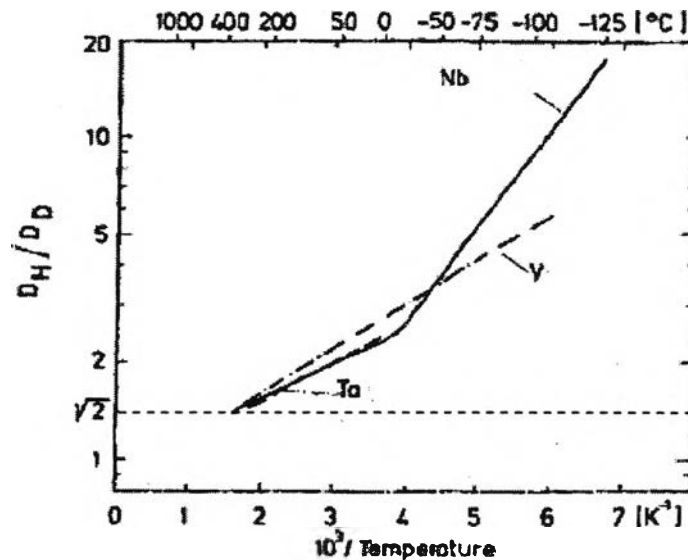


**Figure 2.15** Ratios of diffusion coefficients of hydrogen and deuterium in Vanadium (V), Niobium (Nb) and Tantalum (Ta) (Völkl and Alefeld, 1978).

For the fcc metals; Palladium, Nickel and Copper, the pre-exponential factors are mass dependent. The activation energies are mass dependent as well, but, in contrast to the three bcc metals, one finds the activation energy of hydrogen is higher than that of deuterium. This fact leads to deuterium diffusing faster than hydrogen at low temperatures. In Figure 2.16 the ratio of  $D_H/D_D$  for diffusion in Pd from various investigators is shown. In contrast to bcc metals, all values are below  $\sqrt{2}$  and furthermore for  $T < 500^\circ\text{C}$  below 1, indicating the reversed isotope dependence. The tritium-diffusion coefficient follows the same mass dependence as observed for hydrogen and deuterium;  $D_H : D_D : D_T \approx 1 : (\sqrt{2})^{-1} : (\sqrt{3})^{-1}$  for nickel and copper and the activation energies of isotope hydrogen decreases with increasing atomic mass of isotope hydrogen (Völkl and Alefeld, 1978).

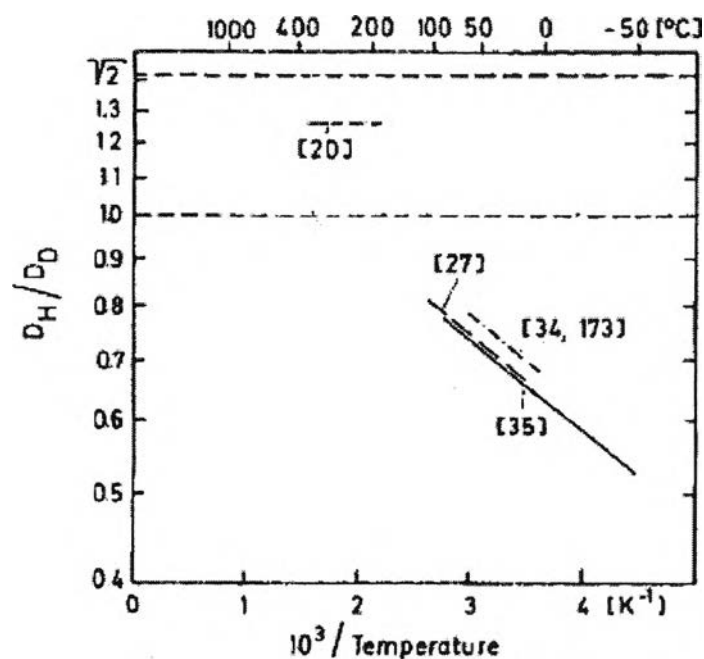


**Figure 2.16** Ratios of diffusion coefficients of hydrogen and deuterium in palladium (Numbers in brackets refer to references of diffusion of hydrogen in metals, Hydrogen in metals I) (Völkl and Alefeld, 1978).

## 2.7 Surface effects

By definition, the permeability and diffusivity of hydrogen in metals are independent of surface conditions as these properties assume diffusion-controlled transport of hydrogen through the lattice. In practice, however, experimental measurements are strongly influenced by surface conditions. Oxides have been proposed as diffusion barriers for austenitic stainless steels used in fusion reactors. These oxides, in some cases, have been shown to significantly reduce the apparent permeability. When these oxides are very thin, the oxide is thought to reduce the kinetics of diatomic hydrogen dissociation on the surface creating a process that is not rate-controlled by diffusion and thus not a true permeability process. The permeability of stainless steel with surface oxides was increased in one study by coating the oxide with palladium. The palladium catalyzes the dissociation of diatomic hydrogen eliminating the kinetic barrier at the surface and establishing

conditions of diffusion-controlled transport of hydrogen. The implication of this observation is that the permeability through the oxide is similar to that in the metal. On the other hand, the permeability is relatively unaffected by thick oxides; the interpretation being that once the oxide layer reaches a critical thickness the layer forms cracks exposing metal surface.

Oxides and surface films may not have a strong effect on steady-state hydrogen transport, in some cases, but may have a substantial effect on hydrogen transport transients and thus diffusivity measurements. In summary, the surface condition can have a profound impact on the measured quantities in permeation studies, particularly the measured diffusivity, thereby introducing errors into the measurements (Marchi *et al.*, 2007).

Miller *et al.*, 1975 studied the permeation rate of hydrogen through alpha iron specimens by means of a highly sensitive steady-state gas permeation technique over a range of hydrogen pressure from 21 torr to 766 torr and over a temperature range of 342 to 619 K. Both sides of the specimen was coated with a thin activated palladium layer by a vapor deposit of 99.95 percent pure palladium, approximately 1000Å to provide a surface which would allow activation by suitable techniques. Due to the very high rate of diffusion of hydrogen through palladium and the extreme thinness of these palladium layers relative to the iron sample, it is felt that these palladium layers should not contribute significantly to the observed permeation kinetics. They found that an iron surface on which palladium has been deposited providing a suitably active surface for the absorption of hydrogen from the gas phase. Permeation of hydrogen gas through an iron membrane with such a surface exhibits a square root dependence on hydrogen inlet pressure given by Sievert's law, which is used as evidence of diffusion control. The diffusivity of hydrogen through alpha iron was determined as a function of absolute temperature (K) as:

$$D = 1.01 \times 10^{-7} \exp\left(\frac{-802.72}{T}\right) \frac{m^2}{s} \quad (2.42)$$

The hydrogen and deuterium transport parameters such as permeability, diffusivity, and solubility in a Pd-25 pct Ag alloy, using a permeation gas phase technique and, additionally, a computer-controlled microbalance system are studied by E. Serra *et al.*, 1997. From the permeation measurements, the constant describing

surface reaction in Pd-25 pct Ag alloy: the surface constants for the adsorption ( $\sigma k_1$ ) and release ( $\sigma k_2$ ) of hydrogen and deuterium are also determined. The measurements cover the temperature range from 323 to 773 K and a pressure range from 1 to  $10^5$  Pa. The Arrhenius expressions for the permeability and diffusivity for Pd-25 pct Ag alloy are as follows.

#### Hydrogen

$$P_{(H_2)} = 5.58 \times 10^{-8} \exp\left(\frac{-6,304}{RT}\right) \frac{mol}{m.s.Pa^{0.5}}, \quad (2.43)$$

$$D_{(H_2)} = 3.07 \times 10^{-7} \exp\left(\frac{25,902}{RT}\right) \frac{m^2}{s}, \quad (2.44)$$

#### Deuterium

$$P_{(D_2)} = 3.43 \times 10^{-8} \exp\left(\frac{-6,156}{RT}\right) \frac{mol}{m.s.Pa^{0.5}}, \quad (2.45)$$

$$D_{(D_2)} = 1.87 \times 10^{-7} \exp\left(\frac{-24,685}{RT}\right) \frac{m^2}{s}, \quad (2.46)$$

where  $R$  is 8.314 J/K.mol and  $T$  is the absolute temperature in Kelvin.

The ratio  $P_{(H_2)}/P_{(D_2)}$  decreased from 1.58 to 1.55 with a decrease of the temperature from 773 to 373 K. Thus, the mass effect is a little greater than that of the classical theoretical value of diffusion coefficient ratio  $\sqrt{2} = \sqrt{m_D/m_H}$ . The ratio  $D_{(H_2)}/D_{(D_2)}$  decreased from 1.36 to 1.11 with a decrease of the temperature from 773 to 373 K, and therefore, it is smaller than  $\sqrt{2}$ .

The experimental values of coefficients  $\sigma k_1$  and  $\sigma k_2$  of hydrogen and deuterium in Pd-25 pct Ag alloy are well described by the following equations.

#### Hydrogen

$$\sigma k_{1(H_2)} = 1.7 \times 10^{-2} \exp\left(\frac{-26,294}{RT}\right) \frac{mol}{m^2.s.Pa} \quad (2.47)$$

$$\sigma k_{2(H_2)} = 0.51 \exp\left(\frac{-65,490}{RT}\right) \frac{mol}{m^4.s} \quad (2.48)$$

### Deuterium

$$\sigma k_{1(D_2)} = 1.3 \times 10^{-2} \exp\left(\frac{-24,780}{RT}\right) \frac{\text{mol}}{\text{m}^2 \cdot \text{s} \cdot \text{Pa}} \quad (2.49)$$

$$\sigma k_{2(D_2)} = 0.39 \exp\left(\frac{-61,842}{RT}\right) \frac{\text{mol}}{\text{m}^4 \cdot \text{s}} \quad (2.50)$$

It is known that the metals; copper, silver, and gold, which have filled *d*-bands, have an activation barrier for hydrogen chemisorption (Thomkins, 1978). The activation barrier for adsorption of hydrogen on copper is about 19,300 J/mol (Balooch *et al.*, 1974), and it is of the same order for Pd and therefore in good agreement with the activation energy for chemisorption obtained here.

Bruzzoni *et al.*, 2000 performed permeation experiments to study the hydrogen ingress rate into Pd-plated iron membranes using electrochemical impedance spectroscopy technique. The membranes were coated with electroplated Pd film on the both sides. The permeation technique involves introduction of hydrogen at the entry side of the Pd-plated membrane and detection of hydrogen at the exit side of the membrane. The thin membranes were 0.1 mm in thickness. Due to their low thickness, the passage of hydrogen through the bulk substrate was very fast. Therefore these membranes were suitable for studying surface effects; the effect of Pd film on the hydrogen permeation. The results shows that thin Pd films (in the nanometer range) are more effective for a fast passage of hydrogen than conventional (micrometer range) ones.

Not only has the coating of platinum group metals eliminated the kinetic barrier at the surface due to their catalytic activities but also provide corrosion protection to basis metals especially platinum metal because of high electromotive force (emf). A survey of the literature shows that development activities in electroless coating with platinum metal are inconspicuous at present. However, there are a few available processes for coating platinum on the surface using hydrazine as a reducing agent shown in Table 5 and 6 (Mallory and Hajdu, 1990).

**Table 2.4** Hydrazine bath composition and conditions for platinum coating  
(Rhoda and Vines, 1969)

---

Hydrazine bath for Pt:	
Na <sub>2</sub> Pt(OH) <sub>6</sub> (as Pt), g/L	10
NaOH, g/L	5
Ethylamine, g/L	10
Hydrazine hydrate, g/L	1
Temperature, °C	35
Plating rate	12.7 μm/hr

---

This process patented by Rhoda and Vines is intended primarily to produce catalytically active platinum layers on materials suitable for making, for example, fuel cell electrodes. Examples of such materials include nickel powder and graphite powder impacts. However, with the addition of a suitable stabilizer, the same process is claimed to be usable for producing bright decorative or protective coatings on less noble metals. An example of bath composition yielding such deposits is given in Table 2.4. Ethylamine (or other nitrogen compounds such as EDTA, quinoline, and sulfamate) serves as the stabilizer. The solution of Na<sub>2</sub>Pt(OH)<sub>6</sub> is prepared by boiling a chloroplatinic acid solution with excess NaOH. Hydrazine is added just before the plating is started, and its concentration is maintained by either continuous or intermittent additions during the plating. Hydrazine is not stable in this system. This bath was used to plate platinum on copper, but these materials are also claimed to be plateable: Fe, Mo, Ni, Ag and Ti.



**Table 2.5** Hydrazine bath composition and conditions for platinum coating  
(Torikai *et al.*, 1984)

Hydrazine bath for Pt:	<u>Bath A</u>	<u>Bath B</u>
$(\text{NH}_3)_2\text{Pt}(\text{NO}_2)_2$ , g	0.5	-
$\text{K}_2\text{Pt}(\text{NO}_2)_4$ , g	-	0.6
$\text{NH}_4\text{OH}$ (28% $\text{NH}_3$ ), ml	50	20
$\text{H}_2\text{O}$ , ml	250	100
To the above mixture, add the two components listed below.		
$\text{NH}_2\text{OH}.\text{HCl}$ (50% soln.), ml	10	-
$\text{NH}_2\text{OH}.\text{HCl}$ (solid), g	-	0.2
Hydrazine hydrate (80% $\text{N}_2\text{H}_4$ ), ml	5	3
$\text{H}_2\text{O}$ (to a total volume of), ml	400	200
pH	11.7	11.8
Temperature, °C	40-50	40-50
Plating rate	3 $\mu\text{m}/2\text{hr}$	2.5 $\mu\text{m}/2\text{hr}$
Pt utilization in 2hr	98%	98%

These processes used nitro or nitroammine complexes of platinum to prepare electroless platinum baths containing hydrazine. Hydroxylamine was found to be a very effective stabilizer. Two bath compositions are given in Table 2.5. The baths can be operated at relatively low temperatures, and they are said to have good stability and high utilization efficiency for platinum. The following are listed as plateable substrates: Cu, Ni, Fe, their alloys, Ti, Ta, ABS plastics, polyamide, polycarbonate, glass, ceramics, and ion exchange membranes used for water electrolysis. The deposit is ductile and claimed to be especially suitable for use on flexible materials such as the ion exchange membrane electrode.

## 2.8 Hydrogen Damage

Hydrogen damage is a general term which refers to mechanical damage of a metal caused by the presence of, or interaction with, hydrogen. Hydrogen damage may be classified into four distinct types: Hydrogen blistering, Hydrogen embrittlement, Decarburization and Hydrogen attack (Fontana, 1987).

### 2.8.1 Hydrogen blistering

Hydrogen blistering results from the penetration of hydrogen into a metal. The result is local deformation and, in the extreme cases, completes destruction of the metal. Much of the hydrogen diffuses through the steel and combines to form hydrogen molecules on the exterior surface. If hydrogen atoms diffuse into a void, a common defect in rimmed steels, they combine into molecular hydrogen. Since molecular hydrogen cannot diffuse, the concentration and pressure of hydrogen gas within the void increases. The equilibrium pressure of molecular hydrogen in contact with atomic hydrogen is several hundred thousand atmospheres leading to blister formation, growth and eventual bursting of the blister.

### 2.8.2 Hydrogen embrittlement

Hydrogen embrittlement (HE) is also caused by penetration of atomic hydrogen into the crystal structure of metal. Molecular hydrogen formed at those sites builds-up pressure causing the rupture of the inter-atomic bonds resulting in a loss of ductility and decreasing the cohesive strength, forming voids and blisters which leads to the formation of cracks on the material (Matei, 1999). However, the exact mechanism of hydrogen embrittlement is not as well known as that of hydrogen blistering. For titanium and other strong hydride-forming metals, dissolved hydrogen reacts to form brittle hydride compounds. In other materials, such as iron and steel, the interaction between dissolved hydrogen atoms and the metal is not completely known.

Most of the mechanisms that have been proposed for hydrogen embrittlement are based on slip interference by dissolved hydrogen. This slip

interference may be due to the accumulation of hydrogen near dislocation sites or microvoids, but the precise mechanism is still in doubt.

### 2.8.3 Decarburization and Hydrogen Attack

Decarburization or the removal of carbon from steel is often produced by hydrogen attack at high temperatures. Hydrogen attack refers to the interaction between hydrogen and a component of an alloy at high temperatures. Hydrogen permeated into the steel can react with carbon, resulting in the formation of methane. The methane is more or less trapped in the metal structure and will accumulate in voids in the metal matrix. The gas pressure in these voids can generate an internal stress that is high enough to fissure, crack or blister the steel. This process is known as hydrogen attack and leads to decarburization of the steel resulting in a reduction of tensile strength and an increase in ductility and creep rate. Thus after long-term exposure to hydrogen at elevated temperatures, steels tend to lose their strength.

The cracking of feeder pipes at Point Lepreau Generating Station (PLGS) has been studied but there is no evidence that the cracking was due to hydrogen damage. The investigation indicated that the corrosion is caused mainly by FAC. Thus it is expected that the hydrogen atoms produced by FAC either diffuse through the pipe wall or into the solution. The exact cause of the cracking of these pipes has not been identified.

## 2.9 Hydrogen Effusion Probe (HEP) for Monitoring Corrosion

When the metal surface is exposed to the water, the oxide film formed on the metal surface and hydrogen generated as a consequence of FAC is shown in the reaction below.



This reaction indicates four possible methods of measuring the corrosion rate, i.e., measurement of (a) metal consumed, (b) water consumed, (c) metal oxide formed, and (d) hydrogen formed. Methods (a) and (c) entail difficulties since the limitation of weight gain and weight loss methods are particularly difficult when the corrosion rates are low, and method (b) has not been attempted. Thus a method (d) could be attractive (Bloom and Krulfeld, 1957).

However, there is some available equipment used for measuring the metal consumed or metal loss in the lab (Lister *et al.*, 2000).

### 2.9.1 Wire resistance probes

The wire probe functions on the principle that the resistance of the carbon steel sensing element increases as the cross-sectional area of the sensing element decreases due to corrosion. An in-situ corrosion rate monitor using carbon steel wire, which is the same material used in the feeder pipes in CANDU reactors, has been used as one of the sensing elements. The schematic of wire resistance probe shows in Figure 2.17. CNER's electrical resistance wire probe can be used under the simulated high temperature, high pressure and high flow velocity feeder pipe conditions (LiOH solution, 5 to 20 m/s velocity, 310°C temperature and 10.1 MPa pressure) with a precision in the order of 0.1  $\mu\text{m}$  in terms of thickness change.

The sensing element used is a carbon steel wire, ~100mm length x 1.5mm diameter, which was machined from the wall of carbon steel grade A106-B, 2.5 inches outside diameter. The carbon steel wire is positioned inside a ceramic tube through which the liquid is forced to flow. The resistance of the sensing element is measured in a four-wire mode to eliminate the contribution from the electric leads and is compensated for the temperature variation.

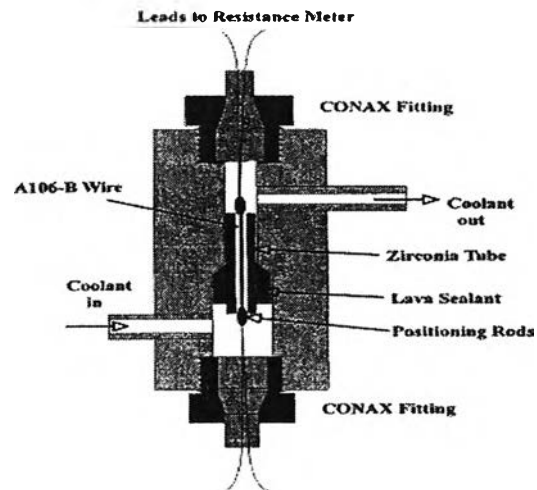


**Figure 2.17** Schematic of the wire resistance probe (Lister *et al.*, 2000).

### 2.9.2 Tube resistance probes

Tube resistance probe is one of the equipment used to monitor corrosion in the UNB test loop. Figure 2.18 shows a drawing of the tube resistance probes assembly. The tubes are constructed of A106-B carbon steel but may be made of any metallic material. The tube resistance probe is connected to the test loop by a Swagelok fitting on one end and a Conex fitting with a Grafoil seal and electrical insulator on the other end. The tube resistance is measured by a 4-wire scheme, to negate any effects from the leads, by a digital multi-meter. The tube resistance measurements along with temperature measurements from the test loop are used to calculate the metal penetration by a Visual Basic computer program as a function of time. This information is used to determine the corrosion rate as the experiment proceeds.

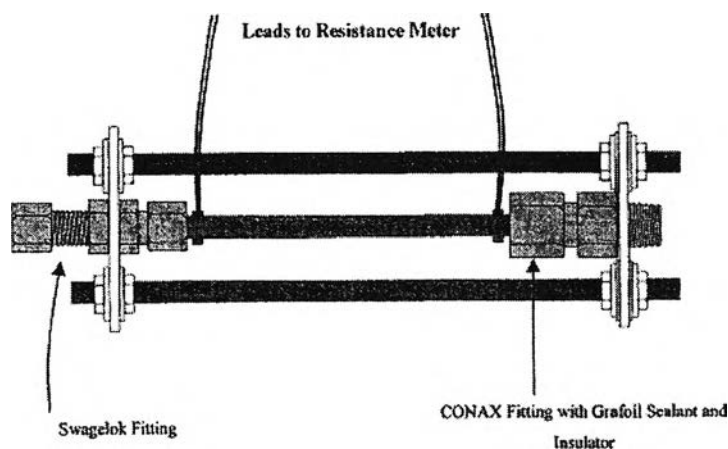


**Figure 2.18** Schematic of the tube resistance probe (Lister *et al.*, 2000).

F. Steward *et al.*, (2000) Centre of Nuclear Energy Research, University of New Brunswick studied an in-situ corrosion rate monitor using a carbon steel tube. A carbon steel rod or a carbon steel wire as the sensing element has been developed. The monitor was tested both in an inert system at room temperature and in a high-temperature and high-pressure loop with LiOH solution. The measured amount of dissolved iron in the solution was compared with the calculated values based on the electrical resistance signal. In some experiments, the diameter of the sensing element was measured with a digital micrometer and comparison was made between the measured and the calculated diameters based on the electrical resistance signal. Experimental results from the room temperature tests shown that the calculated corrosion rate or thinning rate based on the resistance signal of the carbon steel sensing element agreed well with the measured values. So, the resistance signal from a carbon steel sensing element can be used to predict the thinning or corrosion rate of carbon steel specimen. Experimental results obtained from the high-temperature tests shown that the corrosion rate monitor can be applied in the high-temperature, high-pressure and high flow velocity conditions. The precision of the monitor under the simulated nuclear coolant conditions was found to be  $\pm 0.04 \mu\text{m}$  to  $\pm 1 \mu\text{m}$ , depending upon the dimension of the sensing element.

### 2.9.3 Ultrasonic probes (UT)

The Ultrasonic probe is used to monitor corrosion in the UNB FAC loop. The ultrasonic transducer and associated software were provided by the New Brunswick Research and Productivity Council (RPC). A drawing of the Ultrasonic probes assembly is shown in Figure 2.19. The assembly was designed and built in house. It includes titanium housing. An A106-B coupon (or any other suitable material) sits at the top of the assembly. The coolant enters at the bottom of the assembly and flows through an orifice which causes a jet coolant to impinge onto the coupon. A high-temperature ultrasonic transducer is mated externally to the coupon with gold foil to ensure continuous contact between the coupon and transducer. The transducer emits high frequency sound waves which travel through the coupon. The time for the sound waves to travel through the coupon and back from reflection at the metal-coolant interface is measured. Change in the time of travel indicates the coupon change in thickness. The software provided by RPC calculates the thickness of the coupon. This data may be used to obtain metal penetration and corrosion rate as a function of time.

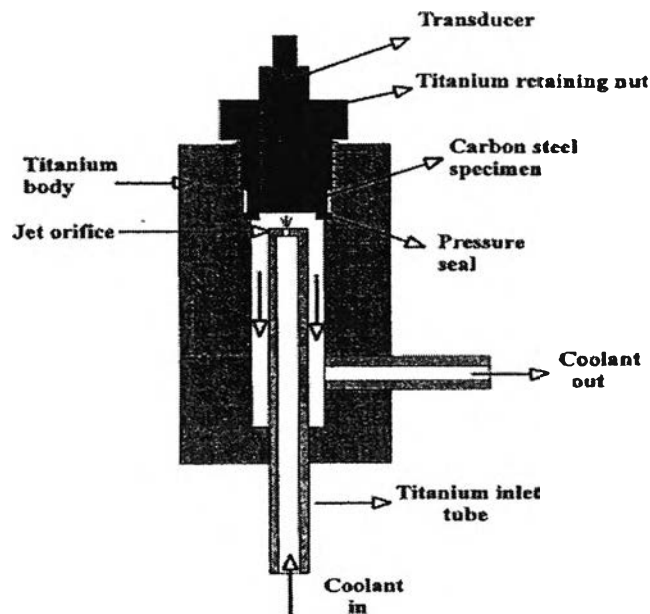


**Figure 2.19** Schematic of the ultrasonic probe (Steward *et al.*, 2000).

#### 2.9.4 Hydrogen Effusion Probe (HEP)

An instrument for measuring the hydrogen generated by the corrosion has been proposed, HEP. The HEP consists of a silver cup, connected via silver and stainless steel tubing to a valve, pressure transducer, vacuum pump and data acquisition system. In order to avoid the leak of hydrogen from the device, high purity silver is used due to the low permeation rate of hydrogen through this metal at high temperature. Thermocouples are installed for measuring the solution temperature to provide temperature information to enable analysis of data. The main components of the HEP instrumentation unit are an isolation valve, a precision absolute pressure transducer, a data acquisition system and a control system. The pressure transducer has a controlled internal temperature of 45°C and a limiting ambient operating temperature of 40°C. Changes in ambient temperature affect the transducer reading. The data acquisition system and the control system are used to control the pump and valve operation and also record readings from the pressure transducer and thermocouples. A schematic of the hydrogen effusion probe components is shown in Figure 2.20. The probe and attached tubing is constructed of silver to minimize the diffusion of captured hydrogen flowing from the internal volume of the equipment (McKeen, 2006).

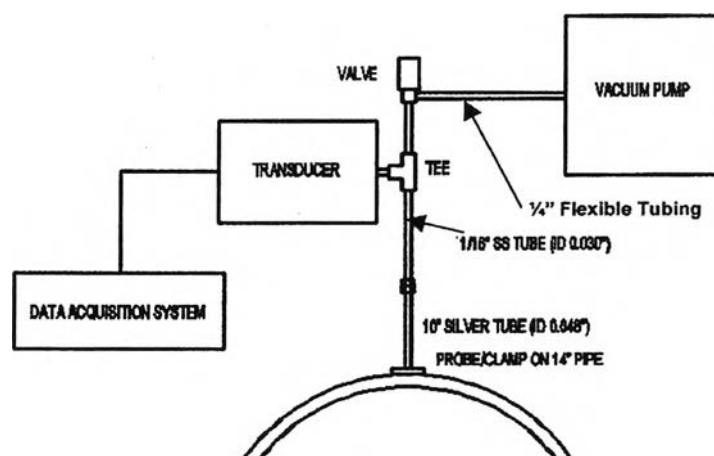


**Figure 2.20** Schematic of the hydrogen effusion probe components (McKeen, 2007).



#### 2.9.4.1 Hydrogen Probe Principle

The concept of the hydrogen effusion probe (HEP) is based on the fact that one of the cathodic reaction products in the corrosion process is hydrogen. The HEP can measure the pipe thinning rate since the quantity of hydrogen effusing through the carbon steel pipe is proportional to the rate that iron is lost into solution as a consequence of FAC and is collected in the chamber outside of the pipe wall which causes the pressure to rise. The pressure transducer measures the hydrogen pressure increase which can be used to calculate the wall thinning rate.

In this method it is assumed that all of the hydrogen liberated in the corrosion reaction diffuses through the pipe wall and one mole of hydrogen gas is produced from one mole of iron reacted. The reaction for this reaction is shown below.



The rate of corrosion is related to hydrogen evolution and can be determined from the accumulation of hydrogen molecules within the chamber according to following equation

$$C_r = \frac{a \frac{\partial n}{\partial t} M_{Fe}}{A_i \rho_{Fe}} \quad , \quad (2.52)$$

where

$C_r$  is the corrosion rate (cm/yr)

$a$  is the conversion of days to year (365 days/yr)

$\frac{\partial n}{\partial t}$  is a daily accumulation of hydrogen molecules  
(moles/day)

$M_{Fe}$  is the molar mass of iron which is 55.85 g/mol

$A_i$  is an internal area of pipe (cm<sup>2</sup>)

$\rho_{Fe}$  is the density of iron which is 7.87 g/cm<sup>3</sup>

Since hydrogen behaves as an ideal gas at low pressure and moderate temperatures, the number of moles of hydrogen accumulation per day can be related to the change in pressure by the Ideal Gas Law.

$$\frac{\partial n}{\partial t} = \frac{\partial P}{\partial t} \frac{V}{RT_{eff}} \quad , \quad (2.53)$$

where

$\frac{\partial P}{\partial t}$  is the rate of pressure increase (Pa/day)

$V$  is the total volume of the HEP which depends on an assembly of the HEP

$R$  is the gas constant ( $8.314 \text{ m}^3 \cdot \text{Pa}/\text{mol} \cdot \text{K}$ )

$T_{eff}$  is the effective temperature (K) in the system.

Since various parts of the HEP system are exposed to different temperatures the effective temperature is the sum of the individual temperatures multiply by their respective volume percentage of the HEP system.

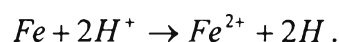
The HEP system operates under vacuum. A vacuum pump is used to create a vacuum within the silver cup, tubing and valve. It was expected that after a predetermined pressure is reached, 2000 Pa is recommended, the data acquisition and control system automatically repeats the test cycle. The vacuum pump switches on to evacuate the measuring volume and restart the cycle (McKeen, 2007).

Since 2001, Atomic Energy of Canada Limited (AECL) has performed a series of loop experiments funded by the CANDU<sup>®</sup> Owners Group Inc. (COG). The objective of this experiment is to study the FAC process that causes feeder wall thinning in the primary heat transport system of CANDU reactors. The results demonstrate that the rate of the FAC process in the tube can be examined online by measuring the rate of hydrogen that is produced, which effuses through the pipe wall. Consequently, this information led to the development of a Hydrogen Effusion Probe (HEP) for monitoring of FAC.

#### 2.9.4.2 Assumptions for Thinning Rate Measurement by the HEP

The requirements for an HEP to be used for the quantitative measurement of FAC rates are as follows (CNER, 2006):

1) The stoichiometric factor relating the rate of atomic hydrogen production to the rate of iron atom oxidation is fixed, and is defined by the reaction,



This means that for every one mole of iron lost, one mole of H<sub>2</sub> is produced.

2) All the atomic hydrogen produced by the FAC process is absorbed locally by the carbon steel experiencing FAC and recombines into molecular hydrogen.

3) All the absorbed hydrogen diffuses through the wall of the carbon steel pipe experiencing FAC, and recombines to molecular hydrogen at the external interface, and passes into the gas phase in contact with the external surface.

4) Molecular hydrogen, once formed within the collection volume does not diffuse back through the pipe wall.

5) Any molecular hydrogen dissolved in the electrolyte coolant does not contribute to the hydrogen flux through the wall of the pipe. All of the hydrogen that effuses through the steel comes from the corrosion reaction.

6) A very low concentration of oxidizing species is present in the coolant.

7) Atomic hydrogen does not accumulate at the grain boundaries or at defects.

8) The area over which collected hydrogen is generated is assumed to be thinning at a uniform rate.

9) The molar mass and density of the carbon steel are assumed to be equal to those of pure iron.

#### 2.9.4.3 Comparing HEP to FOLTM (Conventional Device)

The Feeder On-Line Thickness Monitor (FOLTM) is one of the devices used to measure the feeder thinning rate. The first FOLTM installation at Point Lepreau nuclear station was in January, 1998 to measure feeder wall thickness. It works by using ultrasonic transducers. These transducers can directly measure the wall thickness of the pipe, average fluid temperature and fluid flow. The FOLTM multi-sensor continuously measures wall thinning and fluid temperature and then inputs these parameters in the flow measurement, because flow measurement accuracy relies on pipe internal diameter and fluid temperature.

Both HEP and FOLTM can be used to measure the pipe wall thinning rate, and do not require penetration of the pressure boundary since they are mounted externally. However, the FOLTM and the HEP are based upon different principles. While the FOLTM provides a measurement of feeder wall thickness, the HEP provides a measurement of apparent change in wall thickness.

The signal-to-noise ration of the HEP is much higher than that of the FOLTM. Consequently, the HEP can measure apparent feeder wall thickness rates over much shorter times; hours versus weeks. Thus, unlike the FOLTM, the HEP is capable of monitoring feeder wall thinning rates during short-term operating transients, and is capable of measuring abrupt changes in feeder wall thinning rate. Moreover, the HEP collects hydrogen which diffuses through a pipe wall and provided the system is operating under reducing conditions; this can be directly correlated to the rate of FAC experienced by the pipe wall at that location. This direct measurement of FAC is expected to allow a change to be detected by the HEP an order of magnitude sooner than with the FOLTM.

The Centre for Nuclear Energy Research (CNER) has been conducting HEP experiments. The objective of this project was to design and build on HEP that could be installed on an outlet feeder pipe at the Point Lepreau Generating Station (PLGS) and water wall tubing at the Coleson Cove Generating Station (CC). The HEP and FOLTM were installed on a feeder pipe at PLGS as shown in Figure 2.21. Leak tests of the HEP were performed prior to start-up and leak rates of 5 Pa/day which represents only a 0.25% contribution were determined. Data from the PLGS indicate that the HEP can provide an online measurement of the

feeder wall thinning rate which is approximately  $60 \mu\text{m}/\text{year}$ . This feeder wall thinning rate was compared with the rate measured by the FOLTM, which was installed next to the HEP for the same period of time. The data indicated that the feeder wall thinning rate from both devices was in agreement. Moreover, the data from this experiment also suggest that the HEP is able to detect small changes in the FAC rate over short periods of time.

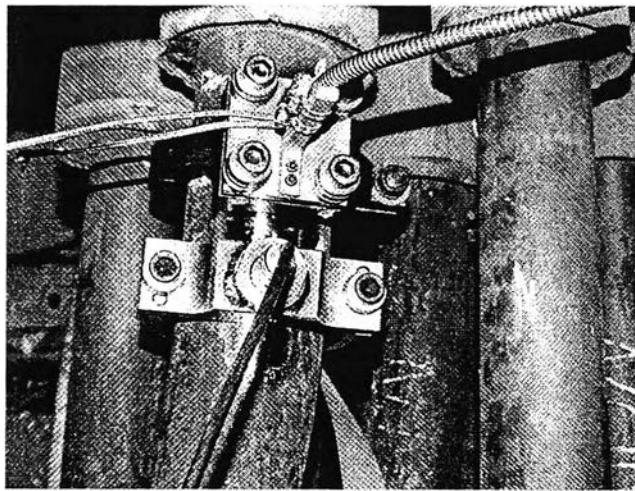


**Figure 2.21** Picture of the HEP (top) and FOLTM (bottom) installed on feeder pipe at PLGS (McKeen, 2007).